Supplement of Atmos. Chem. Phys., 23, 10399–10412, 2023
https://doi.org/10.5194/acp-23-10399-2023-supplement

Atmospheric Chemistry and Physics
Open Access

Supplement of

High potential for CH_4 emission mitigation from oil infrastructure in one of EU's major production regions

Foteini Stavropoulou et al.

Correspondence to: Huilin Chen (huilin.chen@rug.nl) and Thomas Röckmann (t.roeckmann@uu.nl)

Table of Contents

S1. Overview of facility scale quantifications with all methods

Table S1 provides an overview of the number of measurements performed with each quantification approach at different types of production infrastructure during the ROMEO campaign. Most of the quantifications were carried out for oil production sites, and thus the present analysis focuses on this type of sites.

Table S1. Overview of the number of sampled types of sites for each measurement method employed during the ROMEO campaign.

Site Type	Number of sites				
	OTM-33A	GPM[a]	TDM[b]	MBA	Total
Oil production sites	54	68	25	31	178
Gas production sites	11	12	6	2	31
Other facilities[c]	6	30	19	8	63
Unknown	6	1	-	2	9
Total	77	111	50	43	281

OTM-33A: Other Test Method - 33A, GPM: Gaussian Plume Method, TDM: Tracer Dispersion Method, MBA: Mass Balance

[a]This category includes both GPM and “Estimates” based on one mole fraction record.
[b] BDL values estimated from the TDM team are not included in this table (see S2).
[c] ”Other facilities" include oil parks, gas compressor stations, oil deposits, oil and gas production batteries, disposal injection wells and sites mentioned as "other facilities" in the data provided by the O&G production operator.

S2. Facility scale measurement methods

In the following we provide additional information on the deployment of each of the four site level quantification methods during the ROMEO campaign.

Tracer Dispersion Method

The Tracer Dispersion Method (TDM) dataset and the evaluation approach that was implemented during the ROMEO campaign were previously described in Delre et al. (2022).

To release the tracer gas as closely as possible to the emission point, a flexible tube was pushed to the location of the well borehole by using a rod. In cases where this was not possible, such as at large area sources, the tracer was released from the side of the fence protecting the target area. Measurements of CH_4 and tracer gases concentrations were carried out by performing on average 9 downwind plume traverses. The site-representative methane emission rate was then calculated by averaging the emission rates estimated from the multiple traverses across the plume.

Delre et al. (2022) assigned upper limits of emission rates to sites where the measured plumes were Below Detection Limit (BDL). This means that the CH_4 mole fraction downwind a site was the same as upwind, within the analytical uncertainty. Upper limits for emission rates were assigned to these sites based on the lowest measurable emission rate that would have been detectable with the analyser. In this work, these BDL values are not used for the derivation of emission factors with our statistical approach, but they are used for the determination of the detection limit and the fraction of non-detects for the TDM dataset (see S5).

Other Test Method 33A

The Other Test Method (OTM) - 33A dataset and application during the ROMEO campaign was previously described in Korbeń et al., (2022). OTM-33A is based on stationary observations of the mole fraction of trace gases, and quantification using wind direction and speed. When an emission plume has been detected downwind of an emission point from mobile screening (see below), the vehicle is parked in the plume and mole fraction and wind information are recorded over a period of approximately 20 minutes. The CH_4 emission rate Q can then be calculated applying Eq. 1 (Korbeń et al., 2022).

$$Q = 2\pi \cdot \sigma_y \cdot \sigma_z \cdot U \cdot C \quad (1)$$

Where σ_y and σ_z are the horizontal and vertical dispersion coefficients, U is the horizontal mean wind speed, and C is the maximum CH_4 mole fraction calculated with a Gaussian fit algorithm.

Gaussian Plume Method

Measurements with the Gaussian Plume Method (GPM) were additionally performed by the two teams carrying out quantifications using the TDM and OTM-33A approaches as mentioned

in the above sections, and the GPM dataset and application during the ROMEO campaign was also described in detail in (Korbeń et al., 2022) and (Delre et al., 2022).

To determine emission rates from a plume, the GPM calculates the average local-scale CH_4 dispersion using an idealized approximation and assuming constant meteorological conditions (Hanna et al., 1982). When a gas is released from an emission point, it is entrained in the prevailing ambient air flow (defined as the *x* direction) and the dispersion from the emission point creates an idealized cone while it disperses in the *y* and *z* direction over time. The mole fraction of the gas at any point, and eventually the emission rate, can be calculated by using information about the height of the source, wind speed and wind dispersion parameters (Riddick et al., 2017) and applying Eq. 2 (Turner, 1970; Korbeń et al., 2022).

$$C(x,y,z) = \frac{Q}{2\pi\sigma_y\sigma_z U}\exp\left(-\frac{1}{2}\left(\frac{y}{\sigma_y}\right)^2\right)\left[exp\left(-\frac{1}{2}\left(\frac{z-H}{\sigma_z}\right)^2\right) + \exp\left(-\frac{1}{2}\left(\frac{z+H}{\sigma_z}\right)^2\right)\right] \quad (2)$$

where σ_y and σ_z are the horizontal and vertical dispersion coefficients, U is the mean wind speed, and C is the maximum observed CH_4 mole fraction. This method can be used on public roads without site access and measurements can be carried out in a straightforward manner and a limited time. However, GPM modelling can introduce systematic errors that are difficult to quantify and result in errors on emission magnitudes of at least a factor of three, if not more (Yacovitch et al., 2015).

Because of site accessibility and/or wind conditions, some emitting sites could not be successfully quantified using the TDM. In these cases, the emission rates were calculated by fitting a Gaussian peak to the CH_4 enhancement recorded a few meters downwind of the site (conceptually similar to the "screening" evaluations described in section S10). This approach uses often only one single mole fraction record. Emission rates from this approach are referred to as "Estimate" and they are included in the group GPM here. Delre et al. (2022) compared emission rates derived from all three evaluation methods (TDM, GPM, "Estimates") at 41 O&G sites. They found lower estimates from GPM and "Estimate" evaluations compared to TDM and applied a correction of a factor of 2 or more to the GPM and "Estimate" quantifications (Delre et al., 2022). As stated in the main text, we do not apply this correction to GPM measurements, since a comparison to TDM is not possible for the other measurement teams (Korbeń et al., 2022).

On several days of the ROMEO campaign, the C_2H_2 analyser was not operational and the TDM could not be applied. During these days, the GPM was applied by the same team using a CH_4 analyser. Similarly, when the OTM-33A could not be applied, either because the topographic conditions were not suitable or because the wind conditions were not appropriate, the GPM was applied (Korbeń et al., 2022).

Mass Balance Approach

Two different UAV-based systems using a Mass Balance Approach (MBA) were used to quantify the emission rates from the surveyed oil and gas facilities. Due to their adaptability and flexibility, the two UAV-based methods have the advantage of being able to sample at locations that are hard to reach for traditional measurement methods, allowing quick adaptation of the measurement strategy according to changing wind conditions (Andersen et al. 2021; Morales et al. 2022). This possibility of rapid adaptation to changing wind conditions is highly valuable, especially when a large number of sources have to be quantified in a short amount of time, as was the case during the ROMEO measurement campaign. High sensitivity to wind conditions and a relatively short flight time can be seen as a slight drawback of the UAV-based quantifications

since the individual flight represents a brief snapshot of the plume (Morales et al., 2022). Here we describe the differences in the MBA between the active AirCore system from the University of Groningen (UG) and the Quantum Cascade Laser Absorption Spectrometer (QCLAS) from the Swiss Federal Institute for Materials Science and Technology (EMPA).

The UG MBA has been described in Vinković et al. (2022). The total CH_4 flux in grams per second (gs^{-1}) of a source is derived as:

$$Q_{CH_4} = \overline{v}cos\overline{\theta}M_{CH_4}\overline{n}_{dryair}\sum\sum \Delta c\,\Delta x\Delta z\,, \tag{3}$$

where $\overline{v}$ is the mean horizontal wind speed, $\overline{\theta}$ is the angle between the mean wind direction and the flight trajectory, M_{CH_4} is the molecular mass of methane, $\overline{n}_{dryair}$ is the molar density of dry air, Δc is the enhancement of the CH_4 mole fraction above background, and Δx and Δz are the horizontal and the vertical increments of the integration plane, respectively. The background was determined as the 10th percentile of the downwind flight CH_4 measurements as in Vinković et al. (2022). The total uncertainty is derived by error propagation, based upon the variability and uncertainty in each variable of the equation 3.

The EMPA MBA uses a cluster analysis to separate elevated mole fractions from background measurements, and then applies ordinary kriging to each of the two cluster to interpolate the data in space (Morales et al. 2022). The emission rate Q_C (gs^{-1}) is then derived as:

$$Q_C = \int_{y_{min}}^{y_{max}}\int_{0}^{z_{max}} c(y,z)\,u(y,z)\cdot\hat{n}dzdy, \tag{4}$$

Where the y-axis is aligned with the vertical cross-section. The integral over the 2D-plane is approximated in the observations as a discrete summation of CH_4 enhancement $c(y,z)$ multiplied with the component of the horizontal vector $u(y,z)$ normal to the vertical cross-section. The overall error is a function of the two variables c and u. The horizontal wind vector u(y,z), referred to as projected wind in Morales et al. (2022), involved taking the 1 s average normal wind component and projecting it onto the measurement plane by matching the timestamp of the anemometer to the GPS location of the UAV during the time of measurement. The CH_4 background was determined from measurements outside of the plume of interest following the Robust Extract Baseline Signal algorithm (Ruckstuhl et al., 2012).

Both UG and EMPA measured local meteorological conditions using the 3D sonic anemometer placed in the near vicinity of the source at heights of ~ 3 m (UG) and ~ 5 m (EMPA), with a sampling frequency of 10 Hz (UG) and 20 Hz (EMPA). Since the anemometer was placed in close proximity to the investigated source, the wind measurements were assumed to be representative of the conditions encountered by the UAV. The main difference between these two UAV-based MBA approaches lies in their treatment and incorporation of the wind. EMPA's approach clusters measured methane mole fractions before kriging, where the normal wind components of continuous wind measurements were projected onto the drone positions (Morales et al., 2022). In contrast, UG applies the mean wind, observed throughout the flight, uniformly to all measured methane mole fractions (Vinković et al. 2022).

S3. Statistical tests for lognormality

To examine if our sampled data follow a lognormal distribution, we first log-transform the measured site-level emission rates. The Shapiro-Wilk and Lilliefors tests for normality are then used to determine if the log-transformed data are normally distributed. These two tests are appropriate in a situation where the parameters (μ and σ) of the null distribution are unknown. Previous studies have found that the Shapiro-Wilk test is the most powerful normality test and the performance of Lilliefors test is comparable with Shapiro-Wilk test (Razali and Wah, 2011). We perform the tests for the subset of oil production sites including measurements above the detection limit of each method. The null hypothesis for the tests is that the log transformed emissions data comes from a normal distribution, with critical P-value of 0.05. The statistical tests were performed in *Python* using the scientific computation libraries *SciPy* (Virtanen et al., 2020) and *statsmodels* (Seabold and Perktold, 2010).

Table S2 shows the results from both statistical tests for each tested dataset. For the subset of oil production sites, the null hypothesis of lognormality is accepted by both the Shapiro-Wilk and Lilliefors test for all four measurement methods. Therefore, we conclude that for oil production sites, the assumption that the distribution of site-level emissions rates above the detection limit follows a lognormal distribution is valid. For the screenings, the null hypothesis of lognormality is rejected for three out of five datasets. We decide to apply the statistical estimator for the subset of oil production sites to qualitatively compare the results between the quantifications and the screenings. However, we acknowledge that the lognormal distribution might not characterize the distribution from the screenings accurately.

Table S2. Results from the Shapiro-Wilk test and the Lilliefors test of lognormality for each tested dataset.

Grouping	Shapiro – Wilk test		Lilliefors test	
	P-value[a]	Result	P-value[a]	Result
OTM-33A	0.723	Pass	0.229	Pass
GPM	0.177	Pass	0.504	Pass
TDM	0.100	Pass	0.096	Pass
MBA	0.494	Pass	0.682	Pass
All quantifications	0.121	Pass	0.646	Pass
Screenings[b]				
Vehicle 1	0.018	Fail	0.001	Fail
Vehicle 2	0.940	Pass	0.573	Pass
Vehicle 3	0.377	Pass	0.722	Pass
Vehicle 4	0.036	Fail	0.015	Fail
Vehicle 5	0.002	Fail	0.013	Fail
Combined vehicles	0.002	Fail	0.050	Pass

[a]A dataset with P value above 0.05 is considered as evidence for the lognormal distribution of the dataset, indicating that the datasets "pass" the test for lognormality.

[b]Screenings were performed using five different vehicles and results were

separated accordingly into five different datasets.

S4. Determination of emissions distributions and emission factors

In this study, we estimate emissions probability density functions (pdfs) that follow a lognormal distribution using a mathematical approach that has been used in previous publications (Zavala-Araiza et al., 2015, 2018; Alvarez et al., 2018; Robertson et al., 2020). These pdfs are then used to derive representative site-level emission Factors (EF) that consider the effect of the low probability but high-emission sites that describe skewed distributions.

Let *x* be the natural logarithm of CH_4 emissions (in kg h^{-1}) measured at a site. Since *x* is normally distributed, the pdf of observing a single data point *x*, is given by:

$$p(x|\mu,\sigma) = \frac{1}{\sigma\sqrt{2\pi}} e^{-\frac{(x-\mu)^2}{2\sigma^2}} \quad (5)$$

Where μ and σ denote the mean and the standard deviation of the log-transformed data. We define *Φ(x)* as the cumulative standard normal:

$$\Phi(x) = \int_{-\infty}^{x} \frac{1}{\sqrt{2\pi}} e^{-\frac{\partial^2}{2}} d\partial \quad (6)$$

And:

$$\int_{-\infty}^{x} p(\partial|\mu,\sigma)d\partial = \Phi\left(\frac{x-\mu}{\sigma}\right) \quad (7)$$

The natural logarithm of the likelihood function, or log-likelihood function is:

$$l(\mu,\sigma) = S_o ln\Phi\left(\frac{DL-\mu}{\sigma}\right) - S_r ln\sigma - \sum_{i=1}^{S_r} \frac{(x_i-\mu)^2}{2\sigma^2} \quad (8)$$

where *DL* is the Detection Limit, or the lowest detectable emission rate, of each quantification method, S_o is the number of measurements at or below the detection limit and S_r is the number of measurements above the detection limit. The role and significance of selecting the detection limit and the impact of the number of measurements below that limit are discussed in detail in sections S5 and S8.

We use Maximum Likelihood Estimation (MLE) to derive the parameters μ and σ by performing an optimisation routine which maximises Eq. 8. MLE is a popular method that allows us to use the observed data to estimate the parameters of the probability distribution that generated this observed sample. We also use a direct search algorithm to calculate 95 % confidence intervals (CI) by inverting the Likelihood Ratio Test, a statistical test used to compare the goodness of fit between two models (Zavala-Araiza et al., 2015). We can then use the maximum likelihood estimated parameters to derive a central, site-level emission factor on the arithmetic scale, EF, defined as:

$$\mathrm{EF} = e^{\mu+\frac{1}{2}\sigma^2} \quad (9)$$

Emission distributions can be characterized following this approach for sufficiently large sample sizes (i.e., approximately >25 samples; Alvarez et al. 2018). Zavala-Araiza et al. (2015) provides an extensive description of this statistical approach as well as additional variations or constrains of this method.

This statistical estimator approach is our default method for the determination of emissions distributions and emission factors. In addition to the statistical estimator, we use alternative approaches to determine the whole basin emission factor by separating data from each measurement method (OTM-33A, GPM, TDM, MBA) into two regions, referred to as “east” and “west” parts of the production basin (see Fig. 1 in main text). In this approach, the non-detects were added based on the lowest measured value per method and per region (Table S3). In this approach, methods that have measured very low values do not need non-detects. A more detailed description and the results of this approach can be found in Section S7.

S5. “Non-detects” and Detection Limit

To ensure that our emission factor estimates are as representative as possible of the emission distribution of the total population of oil production sites in the studied regions, the implementation of the statistical estimator requires information about the detection limit of each method and the number of sites emitting at an emission rate below this detection limit, the so called "non-detects". The original measurements below the detection limit of each method (if there are any) are replaced by a (typically larger) number of censored data based on the estimated fraction of non-detects (see below).

Korbeń et al. (2022) evaluated data from the screening vehicles to estimate the number of sites below the detection limit for the OTM-33A method. Using a minimum enhancement above background of 200 ppb for the application of the OTM-33A technique, they determined a fraction of 35 % of non-detects for the subset of oil production sites. The detection limit of the OTM-33A has been discussed in previous studies. Brantley et al. (2014) determined the detection limit of OTM-33A method equal to 0.036 kg h^{-1}. Robertson et al. (2020) performed a sensitivity analysis using different detection limits but since no significant effect on the results was found, they also determined the detection limit as 0.036 kg h^{-1}. For the ROMEO measurements, Korbeń et al. (2022) determined the detection limit as 0.11 kg h^{-1}, which is the lowest emission rate measured using OTM-33A in this study. We use this value for our analysis and apply it as well to the GPM dataset because the OTM-33A and GPM measurements were partly carried out by the same teams following a consistent site selection approach (Korbeń et al., 2022).

For the UAV-based measurements, for our reference statistical approach the detection limit is set equal to the lowest quantified value of two UAV-based datasets, which is the same as for the OTM-33A method, 0.11 kg h^{-1}. Since the lowest quantified value of these two measurements methods is the same and they visited approximately the same regions, we also use the same percentage of non-detects as the OTM-33A method, thus 35%. For the alternative statistical approaches A3-A6 (See S7) the detection limit is also set to the lowest quantified value, but per region, which is 0.11 and 0.20 kgh^{-1} for the regions “west” and “east”, respectively. We determine the percentage of non-detects to be equal to 38 % for region “west”, and 55 % for region “east”.

For the TDM quantifications, the number of the BDL sites (see S1) can be directly used as S_0 for the TDM quantifications. This leads to a fraction of 27 % for oil production sites for the TDM method. For the derivation of the detection limit, we use the average of the calculated upper limit emission rates assigned to the sites with emissions BDL. This leads to a detection limit of 0.07 kg h^{-1}. Roscioli et al. (2015) reported the detection limit of TDM equal to 0.02 kg h^{-1}. Because of unfavourable meteorological conditions during the three-week campaign in Romania, in particular low and unstable wind speed, it is reasonable that the detection limit is higher in our study.

We can also use the screening dataset to obtain independent information about the number of sites below the detection limit of our measurement methods. 217 oil production sites had normalized CH_4 enhancements lower than 2.2 ppm, accounting for 32 % of the total number of screened oil production sites that were assigned to the normalized enhancements. As mentioned above, the value of 2.2 ppm is considered as the limit for OTM-33A (Korbeń et al., 2022). For a limit of 1.9 ppm, we get a fraction of 30 %, whereas for a higher limit of 2.5 ppm, we get a fraction of 35 %. These percentages are comparable to the value of 35 % that we used for the derivation of emission factors (for OTM-33A, GPM and MBA), based on the results of Korbeń et al. (2022), and 27 % (for TDM), based on the fraction of BDL values from the TDM team (Delre et al., 2022). An alternative approach to determine the percentage of non-detects for each measurement method using the screening data is described in section see S6.

The effect on the lognormal fit and the final EFs was further evaluated by testing several different values for the detection limit and the fraction of non-detects (see S8). We find that by decreasing the value of the detection limit or by increasing the fraction of non-detects, the estimated EFs increase, due to the widening of the distribution towards the lower end. To avoid overestimating the fraction of non-detects, and thus leading to an erroneously large estimate of the EFs, we perform the calculations with a smaller fraction of non-detects. We consider that a certain portion, specifically 2/3, of the non-detects are zero-emitters, e.g., sites without any emissions. This approach is referred to as our reference scenario (A1) and is discussed in the main text.

Table S3 provides an overview of the different detection limits and percentages of non-detects used for each statistical method A1-A4 that have been performed to evaluate the ROMEO oil production site measurements. Table S10 (section S7) provides an overview of the estimated parameters μ, σ and EF, and a description of these different statistical methods A1-A6.

Table S3. Summary of the different detection limits and percentages of non-detects used for each different approach.

Method	Ref [whole basin]				A3&A4			
	A1		A2		East region		West region	
	DL [kg h^{-1}]	S_o [%]	DL [kg h^{-1}]	S_o [%]	DL [kg h^{-1}]	S_o [%]	DL [kg h^{-1}]	S_o [%]
OTM-33A	0.11	12	0.11	35	0.40	70	0.11	39
GPM	0.11	12	0.11	35	1×10^{-3}	-	0.03	12
TDM	0.07	9	0.07	27	1.2×10^{-3}	-	6.5×10^{-3}	-
MBA	0.11	12	0.11	35	0.20	55	0.11	38

A1-Reference, see section S4, A2-Same as reference approach but with higher # of non-detects, A3-Per method & different # non detects, A4-Per region & different # non-detects, A5-Per method & no non-detects, A6-Per region & no non-detects (A5&A6 use the same DL as A3&A4 but zero S_o and therefore not included separately in the above table). S_o is the number of measurements at or below the detection limit of each measurement method.

S6. Alternative determination of non-detects from screening data

To derive an alternative estimate for the number of non-detects, we investigate the correlation between the CH_4 emission rate determined for the quantified sites and the maximum observed CH_4 mole fraction observed at the same site from the screening data. We expect that in general higher emission rates should correspond to higher mole fractions during the screening phase, but local meteorological conditions will strongly affect the correlation for individual points. Therefore, screenings are not sufficient for an emission quantification since they are short-term observations and not done under controlled and reproducible conditions. In addition, the direct comparison is hampered by the fact that the quantifications and screenings are performed at different times and emissions likely vary over time. Nevertheless, when visiting a lot of sites, the effects of these factors are expected to average out and we use the overall correlation for a statistical analysis. The obtained correlation based on 85 matching pairs has a slope of 0.0196 kg h^{-1} / ppm and a correlation coefficient of $R^2 = 0.53$.

The slope determined from the correlation can be used to roughly estimate (on a statistical basis, not on an individual site basis) emission rates and a probability distribution for an additional set of 883 oil production sites from the screening dataset. When we treat this distribution with our statistical estimator approach, we obtain mean and width of the distribution of as $\mu = -1.81$ and $\sigma = 1.5$. We then use this distribution to attain information about the non-detects (Table S4) for each method (MBA, OTM-33a, GPM, TDM). Defining DL as the lowest emission rate measured for each method and knowing the estimated μ and σ parameters of the distribution through a z-score[1], a percentage of corresponding non-detects was determined for each method by calculating the fraction of values less than that DL. Note that this does not mean that the used methods (MBA, OTM-33a, GPM, TDM) cannot quantify emissions below defined detection limit, only that they generally did not measure emissions below that threshold during the ROMEO campaign.

The investigated basin can also be divided into two regions, i.e., east and west (Fig. 1, main text) and the approach can be performed for the quantifications in both parts individually. Thus, Table S4 gives an overview of parameters together with non-detects for each method (MBA, OTM33a, GPM, TDM) for two different regions (E, W).

Table S4. Overview of parameters for each method (MBA, OTM33a, GPM, TDM) for two different regions, east (E) and west (W).

Method	Region	Nr. Sites	Min = DL [kg h^{-1}]	Max [kg h^{-1}]	S_0 [%]	S_r [nr.]	Total [nr.]	μ	Σ
OTM-33A	E	15	0.40	7.7	30 [70 %]	13	43	-2.06*	2.42*
GPM	E	63	$6x10^{-4}$	39	x [-]**	63	63	-0.21	2.57
TDM	E	19	$12x10^{-4}$	27	x [-]**	19	19	-0.13	2.40
MBA	E	14	0.20	6.5	16 [55 %]	13	29	-1.74*	2.13*
OTM-33A	W	39	0.11	73	24 [39 %]	38	62	-1.05*	2.54*
GPM	W	7	0.03	46	1 [12 %]	6	7	-0.31*	2.84*
TDM	W	8	$65x10^{-4}$	1.5	x [-]**	8	8	-1.47	2.00

[1] $z - score = \frac{\log(x_{min}) - \mu}{\sigma}$

MBA	W	17	0.11	18	10 [38 %]	16	26	-1.19*	2.43*

* μ and σ calculated using the statistical estimator

** no non-detects were added due to very low quantified emissions

DL - detection limit, S_0 - number of measurements equal or below DL, S_r - number of measurements above DL

S7. Alternative up-scaling approaches

Using the alternative approach presented in S6 to determine the non-detects for each method per region, we were able to upscale our emissions to (a) regional and (b) basin-scale. Upscaling is based on the density of normal mixture[1], using the existing function rnormMix from the R package 'EnvStats'. The 95 % CI was determined using the R package 'boot' for a non-parametric bootstrap method (Canty and Ripley, 2021). The main differences between this approach and the statistical estimator method are following:

(i) each measurement method dataset (OTM-33A, GPM, TDM, MBA) is split into two regions (east/west),

(ii) the corresponding percentages of non-detects were added to each measurement method dataset (OTM-33A, GPM, TDM, MBA) according to the lowest regional measured value (Table S5).

The results of the regional analysis and selected groups of methods are presented in Table S5 and Fig. S1. Both regions have similar width of the distribution (Fig. S1), and relatively large 95 % CI due to the small sample size and large variability of the CH_4 emission factor. Nevertheless, we derive comparable estimates in both regions, with a difference of ~ 9 % between the central estimates of 9.9 kg h^{-1} $site^{-1}$ and 9.1 kg h^{-1} $site^{-1}$. When all quantifications from the eastern and western region are combined, we get a central estimate of CH_4 emission level equal to 9.9 kgh^{-1} (7.2 - 14, 95 % CI).

Table S5. Overview of emission factors for the eastern and western part of the basin. Approach referred to as A4.

Method	Region	μ	σ	EF [kg h^{-1} $site^{-1}$]	95 % CI
MBA + OTM-33A	E	-1.87	2.28	2.1	1.6–2.3
GPM + TDM	E	-0.14	2.49	19	14–27
TOTAL E	E	-0.96	2.55	9.9	7.2–14
MBA + OTM-33A	W	-1.09	2.49	7.5	5.5–10
GPM + TDM	W	-0.87	2.53	10	7.0–15
TOTAL W	W	-0.94	2.51	9.1	6.6–13
TOTAL	Whole basin	-0.93	2.54	9.9	7.2–14

[1] $g(x, \mu_1, \sigma_1, \mu_2, \sigma_2) = (1-p)f(x, \mu_1, \sigma_1) + pf(x, \mu_2, \sigma_2)$;
$\mu - mean;\ \sigma - sd; p - mixing\ probability\ vector\ [0.5]$

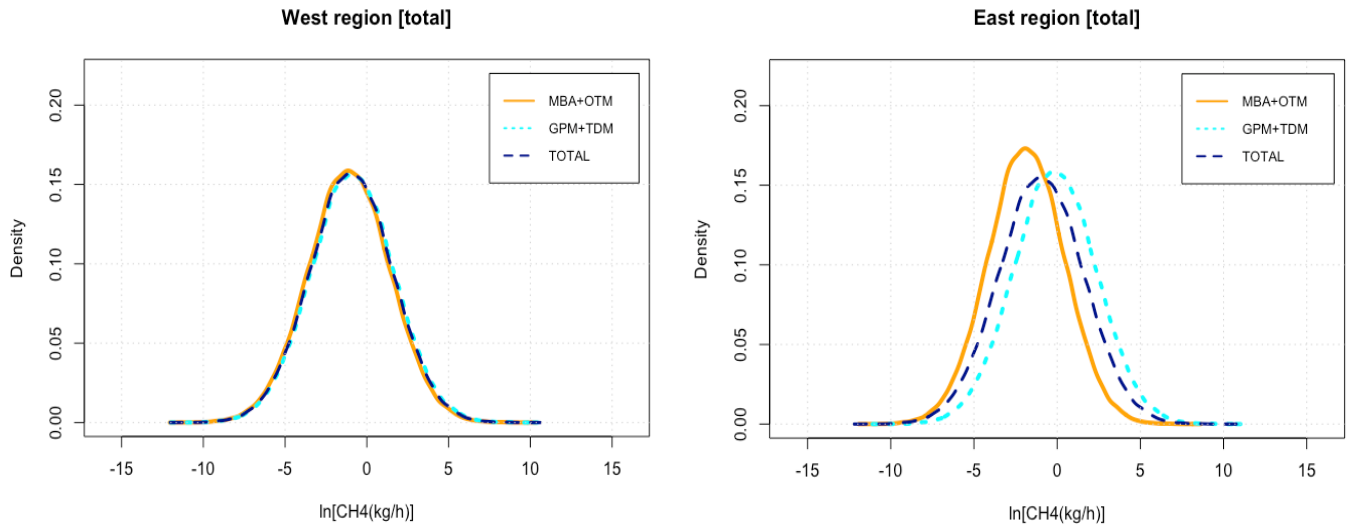

Figure S1. Fitted pdfs for the eastern (a) and western part of the basin (b). The dark blue dashed line presents the total distribution as a mixture of all four quantification methods (MBA, OTM, GPM, TDM) in the eastern and western part, respectively.

Table S6 and Fig. S2 show the results of another alternative statistical approach, where the quantifications are evaluated for the individual methods. The subset of sites evaluated with the GPM method leads to the highest EFs, and the sites evaluated with the MBA to the lowest EFs. The overall basin-wide evaluation of the total set of quantifications again returns an emission factor close to the reference approach, 9.6 kg h^{-1} $site^{-1}$.

Table S6. Summary of the total CH_4 basin emission factors upscaled from the four different measurement methods (OTM-33A, GPM, TDM, MBA). Approach referred to as A3.

Method	μ	σ	EF [kg h^{-1} $site^{-1}$]	95 % CI
OTM-33A	-1.51	2.54	5.6	4.0–7.8
GPM	-0.23	2.71	31	22–46
TDM	-0.78	2.31	6.5	4.9–8.8
MBA	-1.43	2.31	3.4	2.6–4.6
TOTAL	-0.96	2.54	9.6	7.0–14

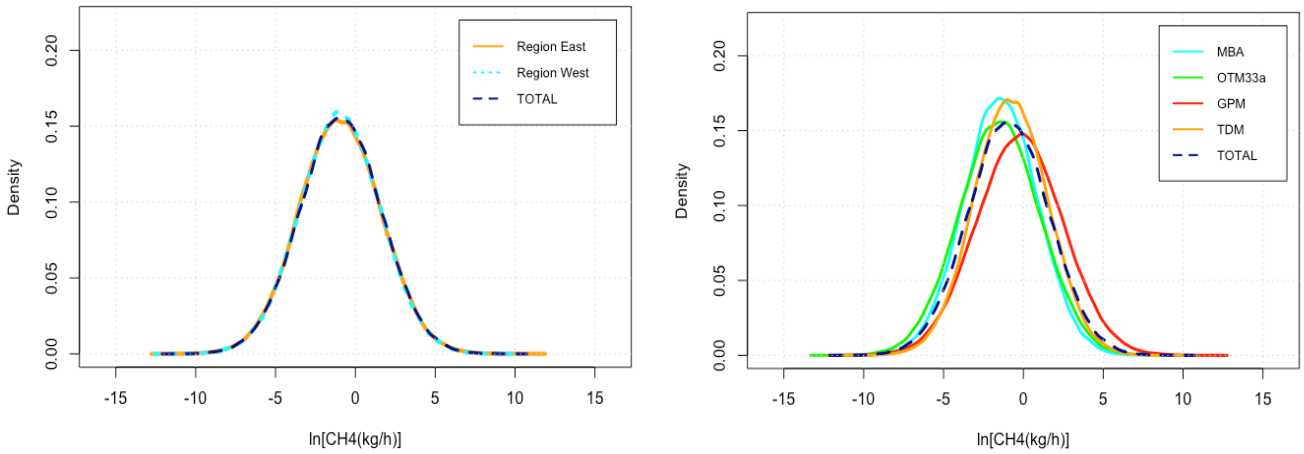

Figure S2. Fitted pdfs derived from the alternative upscaling approaches: per region (left) and measurement method (right). The dark blue dashed line shows the total basin distribution.

Finally, we add a separate mode of zero emitters also for these alternative statistical approaches. This means that instead of adding non-detects to the evaluation with the statistical estimator, we treat the fraction of sites with emission rates BDL as sites that do not emit any CH_4. This is again performed for the entire population of quantifications, for the different regions and the different methods. Results are shown in Table S7 and S8 and Fig. S3.

Table S7. Overview of the total CH_4 basin emission factors per region (east, west) upscaled using the zero-mode approach, referred to as A6.

Region	μ	σ	EF [kg h^{-1} $site^{-1}$]	95 % CI
East	-0.14	1.92	7.3	5.9–9.0
West	-3×10^{-4}	1.97	7.0	5.7–8.7
TOTAL	-0.09	1.95	7.3	5.9–9.1

Table S8. Summary of the total CH_4 basin emission factors per method upscaled using the zero-mode approach, referred to as A5.

Method	μ	σ	EF [kg h^{-1} $site^{-1}$]	95 % CI
OTM-33A	0.65	1.14	3.7	2.4–5.8
GPM	-0.15	2.56	22	8.8–64
TDM	-0.52	2.38	9.8	2.6–46
MBA	0.21	1.22	2.6	1.6–4.3
TOTAL	0.09	1.98	7.8	6.2–10

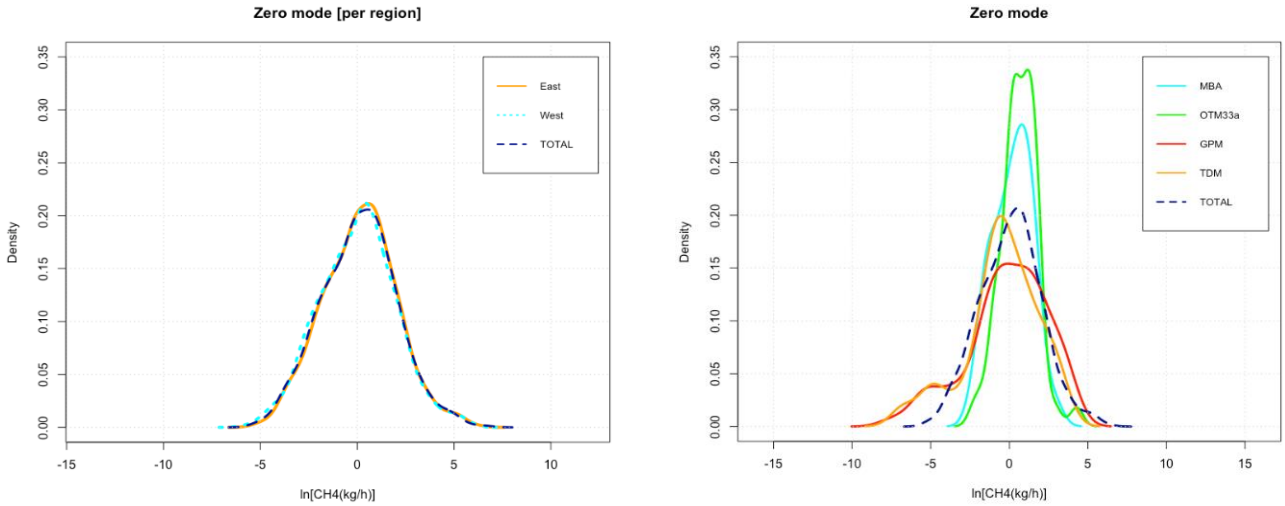

Figure S3. Fitted pdfs derived from the zero-mode upscaling method: per region (left) and measurement method (right). The dark blue dashed line shows the total basin distribution as mixture.

The final additional estimate of the total CH_4 basin EFs is calculated using the reference statistical approach but with a higher fraction of non-detects. This modification of our reference approach uses the original fraction of non-detects discussed in section S5 without assuming a separate mode of zero emitters. Table S9 summarizes the key parameters and derived EFs and Fig. S4 shows the pdfs generated from this modification of the statistical estimator.

Table S9. Summary of parameters from the statistical estimator using a higher fraction of non-detects compared to the reference scenario. Approach referred to as A2.

Method	D_L [kg h^{-1}]	S_r	S_o [% of non-detects]	μ	σ	EF [kg h^{-1} $site^{-1}$]	95 % CI
OTM-33A	0.11	53	29 [35 %]	-0.85	2.38	7.3	2.2–30
GPM	0.11	57	31 [35 %]	-1.00	2.70	14	3.4–74
TDM	0.07	21	8 [27 %]	-0.97	2.46	7.9	1.2–85
MBA	0.11	31	17 [35 %]	-1.07	2.17	3.7	1.0–17
TOTAL	-	-	-	-0.98	2.49	8.3	3.8–19

D_L is the detection limit of each measurement method, S_r is the number of measurements above the detection limit, S_o is the number of measurements at or below the detection limit (included as censored data), EF is the emission factor estimated as $\mathrm{EF} = e^{\mu+\frac{1}{2}\sigma^2}$,TOTAL presents the results of the statistical estimator considering all four measurement methods.

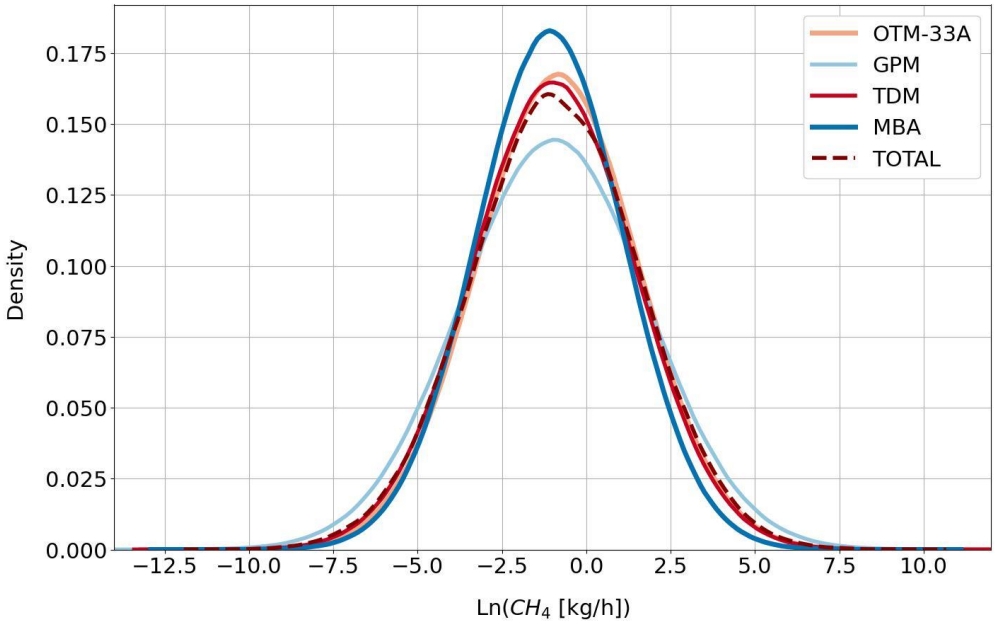

Figure S4. Fitted pdfs of the statistical estimator for each measurement method using a higher fraction of non-detects compared to the reference scenario.

Table S10 and Fig. S5 provide an overview of the different statistical upscaling approaches that have been performed to evaluate the ROMEO oil production site measurements. All estimates agree within the 95 % confidence intervals. Even the lower ends of all individual approaches for oil production sites in the Southern part of Romania from one operator only (still the biggest operator) lead to estimates of the annual emission rate that are larger than the emissions reported by Romania to the UNFCCC for all emissions from oil and gas production, see main text.

Table S10. Different upscaling approaches used to determine the total CH_4 basin emission factors for the ROMEO study.

Approach	Description	EF [kg h^{-1} $site^{-1}$]	95 % CI
A1 (Ref)[a]	Reference scenario	5.4	3.6–8.4
A2[a]	Higher # of non-detects	8.3	3.8–19
A3[b]	Per method & different # non detects	9.6	7.0–14
A4[c]	Per region & different # non-detects	9.9	7.2–14
A2[b]	Per method & no non-detects	7.8	6.2–10
A6[c]	Per region & no non-detects	7.3	5.9–9.1

[a]Overall EFs calculated using the statistical estimator, see S4
[b]Overall EFs calculated by statistically combining the EFs from four methods, see S7
[c]Overall EFs calculated by statistically combining the EFs from two regions, see S7

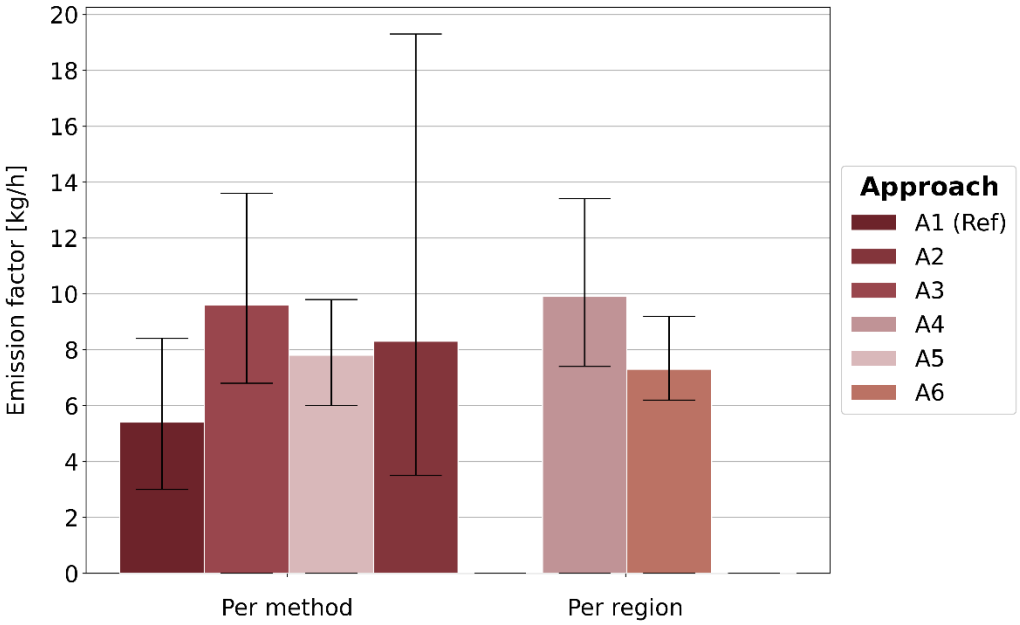

Figure S5. Overview of the CH_4 emission factor calculated from the ROMEO quantifications using the different statistical approaches described above. The error bars represent the 95 % CI of estimated emission factors. The numerical values are reported in Table S9. The approaches differ mainly in the fraction of sites BDL added to the evaluation and the DL of each method. Approaches A5 and A6 do not include any non-detects, but a separate mode of non-emitters.

S8. Sensitivity analysis of the statistical estimator

The results of the statistical estimator depend strongly on two parameters, the detection limit of the measurement method and the number of sites below this detection limit, i.e., the non-detects. We tested the sensitivity of the lognormal fits by running the statistical estimator for three different values for both the detection limit and the fraction of non-detects. We use the subset of oil production sites from the OTM-33A method for the sensitivity analysis. Table S11 provides the summary of the parameters and Fig. S6 presents the fitted pdfs derived from the statistical estimator. By decreasing the value of the detection limit or by increasing the fraction of non-detects, the estimated EFs increase, due to the widening of the distribution towards the lower end. This behaviour is more prominent and results in very large EF estimates when the detection limit is very low. The choice of the detection limit does not affect the high end of the distribution substantially, and the choice of the percentage of non-detects has an even smaller impact. These findings underscore the sensitivity of the statistical estimator to the low end of the distribution and highlight the need for thorough investigation when choosing the values of these two parameters.

Table S11. Summary of parameters from the statistical estimator calculated using different values for the detection limit and for the fraction of non-detects.

Parameter	DL [kg h^{-1}]	S_r	S_o [%]	μ	σ	EF [kg h^{-1} $site^{-1}$]	95 % CI
Detection limit	0.036	54	29 [35%]	-1.39	3.06	27.2	4.4 – 235
	0.11	53	29 [35%]	-0.85	2.38	7.3	2.2 – 30
	0.2	52	28 [35%]	-0.52	2.01	4.5	1.8 – 13
% of non-detects	0.11	53	18 [25%]	-0.31	2.03	5.7	2.3 – 16
	0.11	53	29 [35%]	-0.85	2.38	7.3	2.2 – 30
	0.11	53	43 [45%]	-1.47	2.73	9.7	2.1 – 57

DL is the detection limit of each measurement method, S_r is the number of measurements above the DL, S_o is the number of measurements at or below the DL (included as censored data), EF is the emission factor estimated as $\mathrm{EF} = e^{\mu+\frac{1}{2}\sigma^2}$

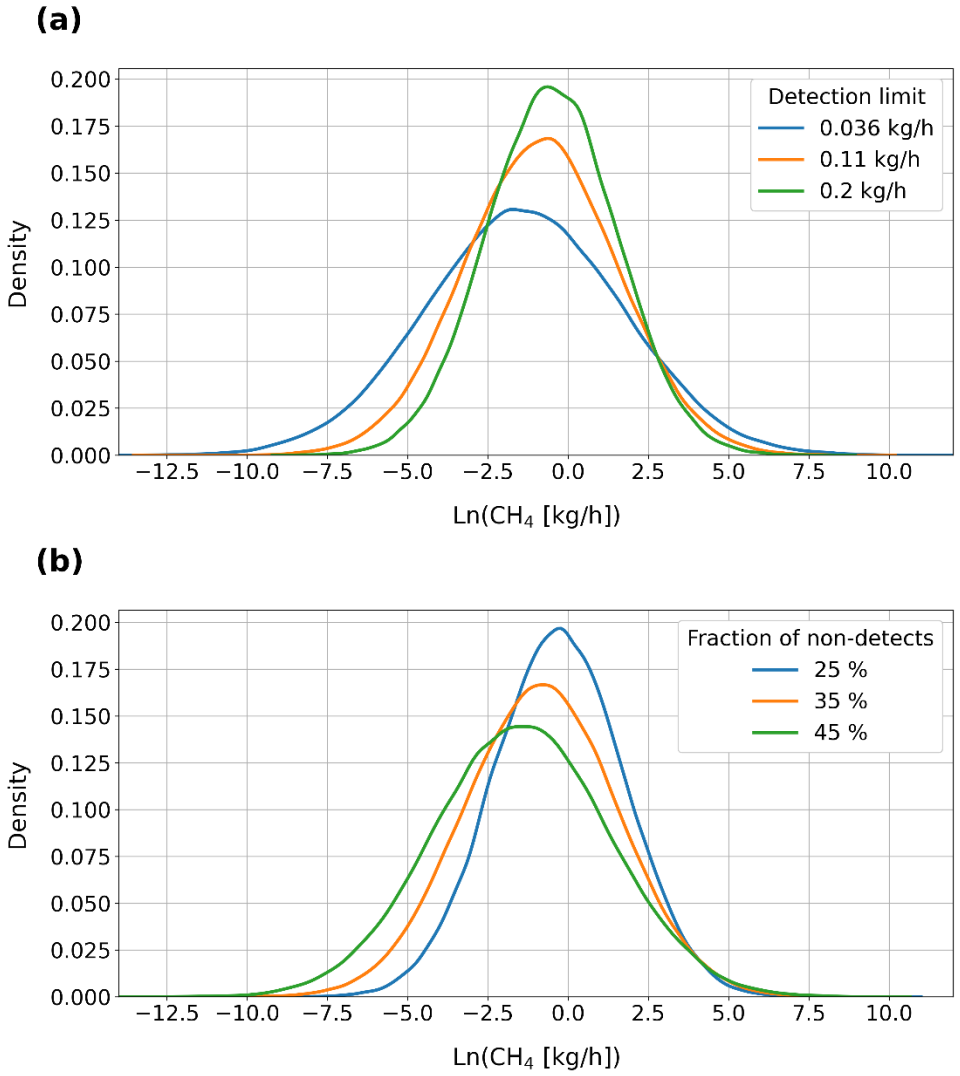

Figure S6. Probability density functions derived from the statistical estimator calculated using different values for the detection limit (top) and number of non-detects (bottom).

S9. Histograms and fitted pdfs under the statistical estimator for each measurement method used

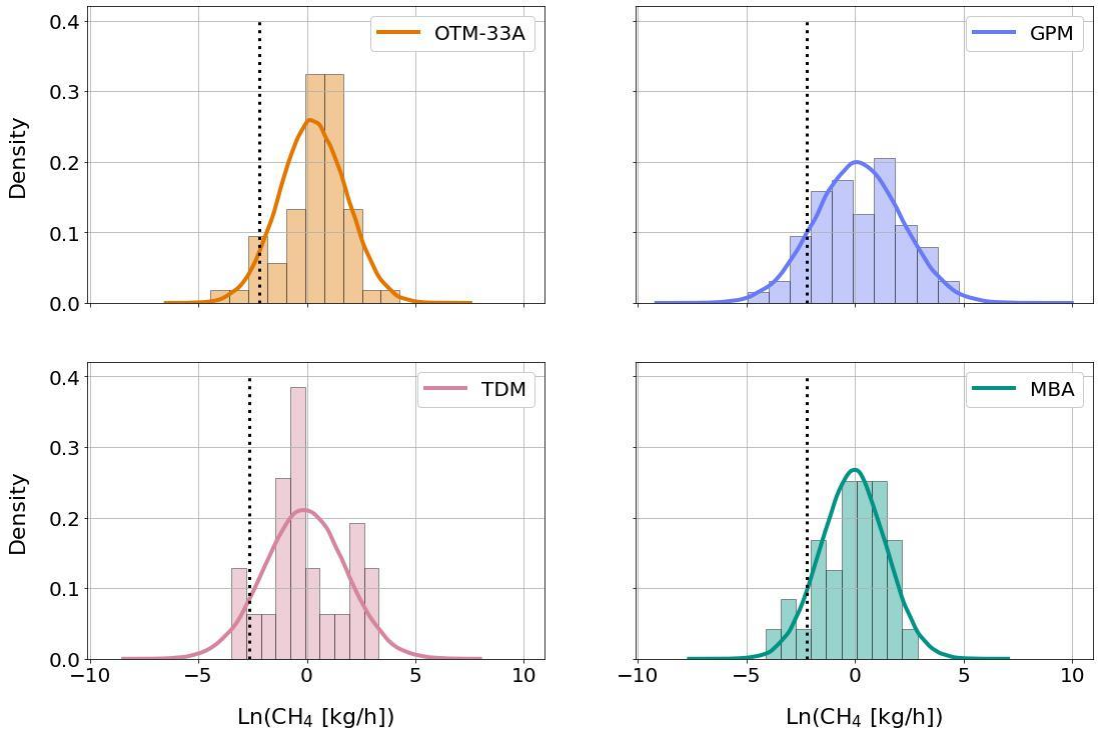

Figure S7. Histograms and fitted pdfs under the statistical estimator for each measurement method used for the reference scenario. Vertical lines indicate the detection limit of each method. Values below these detection limits are the censored data chosen randomly between 0 kg h^{-1} and each method's detection limit and added to the lower end of the distributions to include the non-detects as described in sections S4 and S5.

S10. Semi-quantitative evaluation of screening data

A simplified Gaussian plume algorithm was applied to the screening data from all vehicles to locate the sources and determine normalized CH_4 enhancements. When a CH_4 enhancement was detected, the algorithm looked for registered O&G production sites within a radius of 100 m from the maximum CH_4 mole fraction observed and assigned the emission to this particular site. Gaussian peaks were fitted to the observed data and scaled to 1 m width by conserving the shape of the Gaussian function. This was done because sites were screened from a variety of distances and the maximum signal is not representative for the actual emissions. Scaling the peaks to a common width, which effectively means common distance if the meteorological conditions are similar, allowed to compare normalized CH_4 enhancements of all plumes. Histograms of the normalized CH_4 enhancements from each vehicle performing the screenings and the combination of their datasets are shown in Fig. S8.

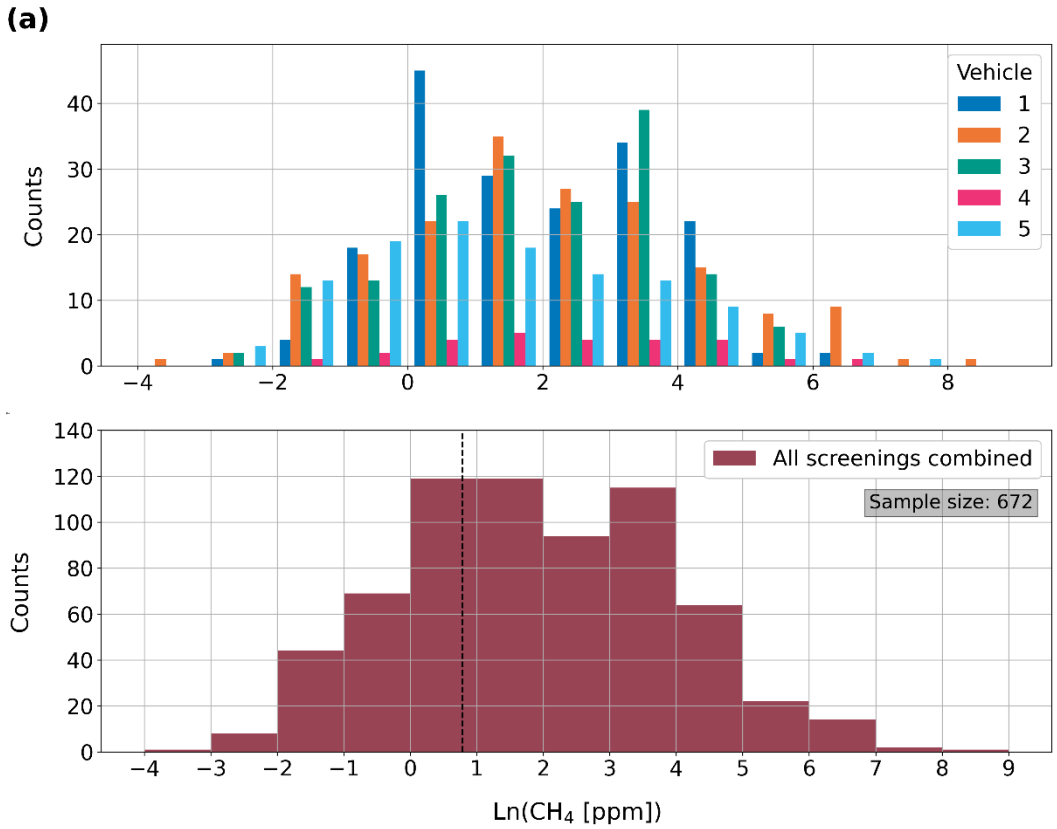

Figure S8. Frequency distribution of normalized CH_4 enhancements for oil production sites from a) different screening vehicles, b) the combination of datasets from the five screenings vehicles. The black dashed vertical line in the lower graph indicates the detection limit of 2.2 ppm used for the OTM-33A dataset.

Table S12 shows the number of successfully normalized CH_4 enhancements from the screening, and parameters μ and σ derived from the statistical estimator using the normalized CH_4 enhancements from each vehicle performing the screenings and the combination of their datasets. When we fit the screening datasets to lognormal distributions, the estimated values for the width of the distributions, σ, range between 1.8 and 2.3 in logarithmic scale, with a total value of 2.0. Here, we assume that the emissions distribution for the screenings is complete, i.e., we do not add measurements below the detection limit. For the quantifications using the Reference scenario and including a small fraction of 9-12 % of non-detects to the distributions, the values for the parameter σ range between 1.5 and 2.0, with a total value of 1.8. We find that the estimates for the width of the distributions converge with the quantifications showing slightly narrower distributions compared to the screenings. However, we note that the estimated parameters under the statistical estimator may not accurately characterize the screening distributions since not all screening datasets passed the statistical tests for lognormality (see S3). Another reason for this small discrepancy could be the effect of the fraction of non-detects to the width of the distribution. As discussed in Section S8, the width of the lognormal fit depends on the choice of the fraction of non-detects and the detection limit.

Table S12. Overview of the number of normalized CH_4 enhancements, and parameters μ and σ derived from the statistical estimator using the normalized CH_4 enhancements per vehicle used for the screenings.

Vehicle[a]	# of Normalized CH_4 Enhancements	μ	σ
1	181	2.0	1.8
2	26	2.3	1.9
3	177	2.1	2.3
4	169	1.9	1.8
5	119	1.4	2.2
Total	672	1.9	2.0

[a]Screenings were performed using five different cars and results were separated into five different datasets.

S11. Component scale measurements

Optical Gas Imaging (OGI, (Lyman et al., 2019)) was used to locate CH_4 sources on the component scale. After the detection and location of leaks with OGI, CH_4 emissions from accessible leaks were measured with a Hi-Flow Sampler (HFS, (Bacharach, 2015)). The HFS is a portable, battery-operated instrument used to determine the rate of gas leakage from individual components in the O&G infrastructure. The component is enclosed in a bag and the gas emitted from the component as well as a certain amount of surrounding air is pumped at high flow rate to a CH_4 analyzer. The gas leak rate of the component can then be calculated using the flow rate of the sampling stream and the gas mole fraction within that stream.

A total of 231 individual leaks were identified with the OGI camera. Because of limited site access, the emission rates of only 62 leaking components were measured using the HFS method. The majority of those, namely 33 leaks, were from two screened gas compressor stations with high number of emission points (see main text) and their emission rates ranged between 0.02 kg h^{-1} to 1.6 kg h^{-1} per leak. From oil production sites, we could only measure leak rates from 14 components using the HFS method, yielding emission rate estimates between 0.1 and 6.5 kg h^{-1} per leak. We note that a site can have several leaking components, which may not all be quantified, resulting in an underestimate of site-level emissions when only the quantified components are considered.

Tab. S13. Overview of the sites screened with infrared camera.

Site Description	# of emitting sites	# of emitting sites	# of identified leaks	# of quantified leaks	Range of CH_4 emission rates [kg h^{-1} $leak^{-1}$]
Oil production sites	155	74	86	14	0.09 - 6.5
Gas production sites	6	3	3	3	0.07 - 0.2
Oil parks	5	5	28	7	0.21 - 6.5
Gas compressor stations	2	2	85	33	0.02 - 1.6
Other Facilities[a]	13	6	30	5	0.14 - 0.6
Total	181	89	231	62	0.07 - 6.5

[a] "Other facilities" include oil production batteries, disposal injection wells, oil deposits, random locations and sites mentioned as "other facilities" in the data provided by the O&G production operators.

S12. Comparison with CH_4 emissions reported from other studies

Table S14. Summary of estimated parameters derived from the statistical estimator for each of the production regions used in our comparison.

Dataset	μ	σ	EF [kg h^{-1} $site^{-1}$]	Gini coefficient[a]	Reference
Denver - Julesburg (Colorado, US)	-0.62	1.3	1.2	0.63	Robertson et al. (2017)
Barnett Shale (Texas, US)	-1.8	2.2	1.8	0.88	Zavala-Araiza et al. (2015)
Red Deer (Alberta, Canada)	-0.31	1.5	2.2	0.70	Zavala-Araiza et al. (2018)
Upper Green River (US)	0.32	1.0	2.4	0.53	Robertson et al. (2017)
Fayetteville (Arkansas, US)	-2.1	2.5	2.5	0.92	Robertson et al. (2017)
Uintah (Wyoming, US)	0.17	1.3	2.7	0.63	Robertson et al. (2017)
Romania (Europe)	0.12	1.8	5.4	0.79	This study
Marcellus (US)	0.39	1.8	7.3	0.79	Omara et al. (2016)
Permian (Texas, New Mexico, US)	1.5	1.1	8.2	0.56	Robertson et al. (2020)
Compressor stations (national, US)	3.1	1.5	64	0.71	Zavala-Araiza et al. (2015)
Processing plants (national US)	4.4	1.3	190	0.64	Zavala-Araiza et al. (2015)

[a]The Gini coefficient is a measure of statistical dispersion used to estimate the inequality among values of a frequency distribution. A Gini coefficient of 0 represents complete equality, whereas a Gini coefficient close to one expresses the maximum inequality among values where a few sites have a highly disproportionate contribution to total emissions.

S13. Production and age characteristics of surveyed oil production sites

To assess how representative the measured oil production sites were in comparison to the characteristics of the total population of oil production sites in Romania and to determine possible differences between the characteristics of oil production sites measured with different quantification methods, we investigated the relation of emission rate with age, oil and gas production provided by the operator. Note that the data provided by the operator regarding oil and gas production solely refers to the three-week duration of the measurement campaign and does not cover the entire year. For the majority of oil production sites visited, the operator reported zero gas production or no gas production for the duration of the measurement

campaign in 2019. For the oil production sites which report a non-zero value for gas production, we calculate the average gas production per site. We use the reported spud dates from the operators to determine the number of years that a particular equipment has been in operation. This analysis was performed for both the component and the facility scale measurements.

A summary of the characteristics for the measured oil production sites and for the total population of oil production sites in Romania is shown in Table S14. The distribution for average site age shows little variability across the different methods, between 28 years for the sites quantified with OTM-33A and 34 years for TDM. The average age of the complete population is 37 years, so the sites targeted during ROMEO were slightly younger than the average age of the total population.

The diversity of the sampled oil production sites is more prominent in terms of production characteristics, and higher than the total population average of 32 tons. Among all measurement methods, TDM sites had the lowest average oil production of 43 tons, followed closely by MBA with 47 tons. GPM had the highest production of 77 tons of oil, more than double the country average value. For the gas production, around 50 % of the sampled oil production sites with OTM-33A, GPM and MBA report zero gas production or had no gas production in 2019, for the TDM this value is 60 %. These percentages are comparable to the 52 % of the total population of oil production sites in Romania. For the sites which report a non-zero value for gas production, TDM was deployed at sites with the highest average production of around 106,000 scm of natural gas, whereas for GPM it was 12,000 scm. The total population average is 27,400 scm. In summary, oil production sites sampled during ROMEO have higher oil production than the total population. In terms of gas production, OTM-33A measurements were representative of the total population of oil production sites. TDM and MBA leaned towards the high, whereas GPM towards the low end of the spectrum.

Table S14. Summary of characteristics (average production and age) from sampled oil production sites based on the measurement method used, and from the total population of oil production sites in Romania. The values related to oil and gas production refer to the production that occurred during the three-week duration of the measurement campaign.

Characteristics	OTM-33A	GPM	TDM	MBA	Total population
Age [years]	28	29	34	30	37
Gas production [10^3 scm]	26	12	106	49	27
Zero gas production [% of sites]	49	51	60	53	52
Oil production [tons]	61	77	43	47	32

Similarly, a summary of the characteristics from the IR screened oil production sites and from the total population of oil production sites in Romania is shown in Table S15. We find that emitting oil production sites have a slightly higher gas production and a lower fraction of wells reporting zero gas production compared to non-emitting oil production sites. For the gas production, approximately 70 % of emitting and 82 % of non-emitting oil production sites visited report zero gas production or had no gas production in 2019. These percentages are higher than the average percentage of the total population of oil production sites in the country. Emitting oil production sites had an average age of 36 years, average gas production of 9,500 scm per and average oil production of 48 tons. We found a slightly lower range of values for non-emitting oil production sites (see Table S15). Overall, the sites visited were representative of the total

574 population of sites in the country in terms of age. However, measurements leaned more towards
575 the high oil, but very low gas producing end of the spectrum.

576 Table S15. Summary of characteristics (average production and age) from screened oil production sites
577 and from the total population of oil production sites in Romania. The values related to oil and gas
578 production refer to the production that occurred during the three-week duration of the measurement
579 campaign.

Characteristics	Emitting oil production sites	Non-emitting oil production sites	Total population
Age [years]	36	37	37
Gas production [10^3 scm]	9.5	7.5	27
Zero gas production [% of sites]	70	82	52
Oil production [tons]	48	52	32

580
581

582 ## S14. Complete quantified emissions dataset

583 Table S16. Emission dataset used in this study

N	Method	Site ID	Region	Site Description	CH_4 emissions [kg h^{-1}]
1	TDM	58	C7	Facility	106.767
2	TDM	7	C8	Gas well	90.439
3	TDM	1	C6	Gas well	66.806
4	TDM	16	C6	Oil well	27.286
5	TDM	45	C6	Facility	25.025
6	TDM	67	C5A	Facility	22.518
7	TDM	59	C7	Oil well	20.071
8	TDM	12	C7	Gas manifold	18.732
9	TDM	48	C7	Oil park	13.030
10	TDM	15	C6	Oil well	11.559
11	TDM	47	C7	Facility	10.692
12	TDM	54	C7	Facility	9.990
13	TDM	18	C7	Oil well	9.537
14	TDM	70	C5A	Facility	8.345
15	TDM	11	C8	Facility	8.313
16	TDM	9	C8	Gas manifold	7.500
17	TDM	13	C7	Oil park	7.118
18	TDM	68	C5A	Oil park	6.442
19	TDM	17	C7	Oil well	6.440
20	TDM	66	C6	Oil park	6.111
21	TDM	74	C5A	Facility	5.028
22	TDM	5	C8	Gas manifold	4.431
23	TDM	44	C6	Oil park	3.983
24	TDM	51/52/53	C7	Oil well	8.275*
25	TDM	2	C6	Oil well	2.580
26	TDM	33	C5A	Oil well	1.463

27	TDM	10	C8	Gas well	1.322
28	TDM	14	C7	Oil well	1.281
29	TDM	69	C5A	Facility	0.833
30	TDM	32	C5A	Oil well	0.816
31	TDM	38	C5A	Oil well	0.778
32	TDM	6	C8	Gas well	0.616
33	TDM	31	C5A	Oil well	0.568
34	TDM	36	C5A	Oil well	0.542
35	TDM	37	C5A	Oil well	0.495
36	TDM	65	C6	Oil well	0.488
37	TDM	42	C7	Oil well	0.443
38	TDM	62	C7	Oil well	0.324
39	TDM	43	C7	Oil well	0.289
40	TDM	4	C8	Oil well	0.245
41	TDM	46	C6	Oil park	0.192
42	TDM	8	C8	Gas well	0.149
43	TDM	60	C7	Facility	0.142
44	TDM	3	C7	Oil well	0.134
45	TDM	55	C7	Oil well	0.118
46	TDM	41	C7	Gas well	0.075
47	TDM	49	C7	Oil well	0.035
48	TDM	40	C5A	Oil well	0.009
49	TDM	39	C5A	Oil well	0.006
50	TDM	75	C7	Oil well	0.001
51	OTM-33A	258	4	Oil well	72.612
52	OTM-33A	279	8	Oil park	33.660
53	OTM-33A	226	4	Oil well	18.432
54	OTM-33A	239	6	Gas well	15.408
55	OTM-33A	263	6	Gas well	14.652
56	OTM-33A	250	5A	Oil facility	12.852
57	OTM-33A	251	5A	Oil park	12.708
58	OTM-33A	274	5A	Oil facility	11.376
59	OTM-33A	286	6	Oil well	7.668
60	OTM-33A	272	4	Oil well	6.984
61	OTM-33A	224	5A	Oil well	6.588
62	OTM-33A	277	8	Unknown	6.444
63	OTM-33A	234	7	Oil well	6.264
64	OTM-33A	281	6	Oil well	6.084
65	OTM-33A	235	2	Oil well	5.544
66	OTM-33A	241	5A	Oil well	5.256
67	OTM-33A	222	2	Oil well	5.112
68	OTM-33A	273	5A	Oil facility	4.932
69	OTM-33A	280	8	Unknown	4.788
70	OTM-33A	232	5A	Oil well	4.680
71	OTM-33A	240	5A	Oil well	4.608
72	OTM-33A	285	6	Oil well	4.392
73	OTM-33A	238	5A	Oil well	4.140
74	OTM-33A	227	4	Oil well	4.068

75	OTM-33A	248	2	Oil well	3.564
76	OTM-33A	295	6	Oil well	3.564
77	OTM-33A	266	5A	Oil well	3.168
78	OTM-33A	249	5A	Oil well	3.132
79	OTM-33A	291	7	Oil well	3.024
80	OTM-33A	231	4	Oil well	2.808
81	OTM-33A	267	4	Oil well	2.736
82	OTM-33A	289	6	Oil well	2.736
83	OTM-33A	228	4	Oil well	2.664
84	OTM-33A	265	5A	Oil well	2.520
85	OTM-33A	229	5A	Oil well	2.412
86	OTM-33A	223	5A	Oil well	1.980
87	OTM-33A	247	5A	Oil well	1.728
88	OTM-33A	252	7	Gas well	1.728
89	OTM-33A	293	6	Oil well	1.692
90	OTM-33A	287	6	Oil well	1.512
91	OTM-33A	288	6	Oil well	1.512
92	OTM-33A	242	2	Oil well	1.476
93	OTM-33A	225	4	Oil well	1.440
94	OTM-33A	259	4	Oil well	1.368
95	OTM-33A	256	4	Oil well	1.332
96	OTM-33A	268	5A	Oil well	1.260
97	OTM-33A	233	5A	Oil well	1.188
98	OTM-33A	294	6	Oil well	1.188
99	OTM-33A	255	5A	Oil well	1.044
100	OTM-33A	269	5A	Oil well	1.044
101	OTM-33A	284	7	Oil well	1.044
102	OTM-33A	221	2	Gas well	1.008
103	OTM-33A	253	5A	Oil well	0.972
104	OTM-33A	264	4	Oil well	0.972
105	OTM-33A	296	6	Oil park	0.936
106	OTM-33A	246	2	Oil well	0.828
107	OTM-33A	290	6	Unknown	0.828
108	OTM-33A	270	4	Oil well	0.792
109	OTM-33A	236	6	Gas well	0.612
110	OTM-33A	261	4	Oil well	0.540
111	OTM-33A	244	2	Gas well	0.504
112	OTM-33A	262	5A	Oil well	0.504
113	OTM-33A	276	8	Unknown	0.504
114	OTM-33A	230	2	Gas well	0.432
115	OTM-33A	260	5A	Oil well	0.432
116	OTM-33A	282	6	Oil well	0.432
117	OTM-33A	297	6	Oil well	0.396
118	OTM-33A	275	6	Oil well	0.360
119	OTM-33A	245	2	Gas well	0.324
120	OTM-33A	271	5A	Oil well	0.324
121	OTM-33A	283	7	Unknown	0.252
122	OTM-33A	243	2	Gas well	0.180

123	OTM-33A	254	5A	Oil well	0.180
124	OTM-33A	278	8	Gas well	0.180
125	OTM-33A	292	7	Unknown	0.180
126	OTM-33A	237	2	Gas well	0.108
127	OTM-33A	257	4	Oil well	0.108
128	GPM	50	C7	Oil park	138.513
129	GPM	217	7	Oil deposit	93.060
130	GPM	64	C6	Facility	63.771
131	GPM	71	C5A	Oil well	46.069
132	GPM	24/25/26	C6	Oil well	118.079*
133	GPM	56	C7	Facility	36.660
134	GPM	212	4	Other facility	31.176
135	GPM	21	C7	Oil well	26.487
136	GPM	201	4	Oil well	25.920
137	GPM	23	C6	Oil well	22.722
138	GPM	220	5A	Unknown	14.904
139	GPM	57	C7	Facility	14.655
140	GPM	202	7	Oil well	14.220
141	GPM	219	5A	Gas compressor	12.996
142	GPM	22	C6	Oil well	12.522
143	GPM	211	5A	Oil park	11.952
144	GPM	20	C7	Oil well	10.233
145	GPM	72	C5A	Facility	9.175
146	GPM	19	C7	Oil well	6.649
147	GPM	205	7	Oil well	6.444
148	GPM	61	C7	Facility	6.202
149	GPM	73	C5A	Facility	5.848
150	GPM	213	5A	Oil deposit	5.688
151	GPM	28	C6	Oil well	4.970
152	GPM	27	C6	Oil well	4.416
153	GPM	63	0	Facility	3.812
154	GPM	30	C6	Oil well	3.705
155	GPM	214	5A	Gas compressor	3.204
156	GPM	216	7	Oil deposit	2.484
157	GPM	203	4	Oil well	2.448
158	GPM	215	6	Oil park	1.872
159	GPM	218	7	Oil park	1.656
160	GPM	206	6	Gas well	1.476
161	GPM	29	C6	Oil well	0.956
162	GPM	34	C5A	Oil well	0.731
163	GPM	209	7	Oil well	0.684
164	GPM	210	7	Oil well	0.648
165	GPM	208	7	Oil well	0.576
166	GPM	204	4	Oil well	0.540
167	GPM	207	4	Oil well	0.288
168	GPM	35	C5A	Oil well	0.034
169	Estimate	97	C6	Gas well	61.228
170	Estimate	81	C8	Gas well	33.910

171	Estimate	98	C6	Gas well	31.889
172	Estimate	86	C8	Oil well	22.946
173	Estimate	91	C7	Oil well	19.967
174	Estimate	89	C8	Gas well	15.297
175	Estimate	140	C7	Oil well	7.957
176	Estimate	136	C7	Oil well	6.879
177	Estimate	159	C6	Facility	5.348
178	Estimate	173	C6	Oil well	5.159
179	Estimate	78	C7	Oil well	4.761
180	Estimate	137	C7	Facility	4.332
181	Estimate	155	C6	Oil well	4.100
182	Estimate	149	C6	Oil well	4.041
183	Estimate	93	C7	Oil well	3.696
184	Estimate	95	C7	Oil well	3.432
185	Estimate	152	C6	Oil well	2.944
186	Estimate	94	C7	Oil well	2.904
187	Estimate	96	C6	Gas well	2.551
188	Estimate	90	C8	Oil well	2.550
189	Estimate	88	C8	Facility	2.241
190	Estimate	181	C6	Facility	2.186
191	Estimate	156	C6	Facility	2.165
192	Estimate	82	C8	Gas well	2.118
193	Estimate	138	C7	Oil well	2.087
194	Estimate	84	C8	Gas well	1.540
195	Estimate	158	C6	Oil well	1.425
196	Estimate	180	C6	Oil well	1.343
197	Estimate	79	C6	Oil well	1.199
198	Estimate	143	C7	Oil well	1.196
199	Estimate	170	C6	Oil well	1.172
200	Estimate	141	C7	Oil well	1.120
201	Estimate	162	C6	Gas well	0.862
202	Estimate	147	C7	Oil well	0.849
203	Estimate	176	C6	Facility	0.777
204	Estimate	146	C7	Oil well	0.693
205	Estimate	165	C6	Facility	0.683
206	Estimate	77	C7	Facility	0.538
207	Estimate	153	C6	Oil well	0.536
208	Estimate	83	C8	Gas well	0.458
209	Estimate	76	C6	Facility	0.446
210	Estimate	92	C7	Oil well	0.440
211	Estimate	160	C6	Oil well	0.413
212	Estimate	166	C6	Oil well	0.366
213	Estimate	151	C6	Oil well	0.322
214	Estimate	161	C6	Oil well	0.257
215	Estimate	175	C6	Facility	0.247
216	Estimate	144	C7	Oil well	0.246
217	Estimate	154	C6	Oil well	0.232
218	Estimate	157	C6	Oil well	0.220

219	Estimate	87	C8	Facility	0.215
220	Estimate	135	C7	Oil well	0.210
221	Estimate	171	C6	Oil well	0.175
222	Estimate	179	C6	Oil well	0.167
223	Estimate	139	C7	Oil well	0.165
224	Estimate	148	C6	Facility	0.160
225	Estimate	145	C7	Oil well	0.112
226	Estimate	80	C8	Gas well	0.094
227	Estimate	85	C8	Gas well	0.045
228	Estimate	142	C7	Oil well	0.045
229	Estimate	167	C6	Oil well	0.032
230	Estimate	178	C6	Oil well	0.029
231	Estimate	177	C6	Facility	0.015
232	Estimate	168	C6	Oil well	0.014
233	Estimate	164	C6	Oil well	0.006
234	Estimate	163	C6	Oil well	0.006
235	Estimate	150	C6	Oil well	0.005
236	Estimate	169	C6	Oil well	0.004
237	Estimate	174	C6	Oil well	0.003
238	Estimate	172	C6	Oil well	0.001
239	MBA	318	C8	Oil park	50.640
240	MBA	326	C5A	Oil well	17.593
241	MBA	317	6	Gas facility	9.378
242	MBA	316	7	Oil deposit	7.848
243	MBA	336	C5A	Oil facility	7.526
244	MBA	315	6	Oil well	6.480
245	MBA	339	C5A	Oil well	5.575
246	MBA	314	6	Oil park	5.328
247	MBA	331	C4	Oil well	4.822
248	MBA	330	C5A	Oil well	4.757
249	MBA	313	6	Oil well	4.080
250	MBA	312	6	Oil well	3.618
251	MBA	340	C5A	Oil well	3.331
252	MBA	325	C5A	Oil well	2.943
253	MBA	324	C5A	Oil well	2.630
254	MBA	338	C4	Oil well	2.280
255	MBA	311	6	Oil well	2.148
256	MBA	335	C5A	Oil facility	2.033
257	MBA	337	C4	Unknown	2.032
258	MBA	319	C2	Oil well	1.927
259	MBA	320	C2	Oil well	1.796
260	MBA	310	6	Oil park	1.716
261	MBA	309	8	Oil well	1.710
262	MBA	308	6	Oil well	1.467
263	MBA	307	6	Oil well	1.296
264	MBA	306	8	Oil well	0.960
265	MBA	305	6	Other facility	0.918
266	MBA	304	6	Oil well	0.876

267	MBA	303	6	Oil well	0.846
268	MBA	321	C5A	Oil well	0.831
269	MBA	302	6	Oil well	0.720
270	MBA	327	C5A	Oil well	0.550
271	MBA	301	6	Oil park	0.540
272	MBA	322	C4	Oil well	0.406
273	MBA	342	C5A	Oil well	0.355
274	MBA	300	7	Oil well	0.306
275	MBA	299	6	Oil well	0.252
276	MBA	333	C2	Gas well	0.243
277	MBA	323	C5A	Oil well	0.229
278	MBA	298	7	Oil well	0.198
279	MBA	334	C5A	Oil well	0.196
280	MBA	341	C2	Unknown	0.176
281	MBA	329	C5A	Oil well	0.106
282	MBA	332	C2	Gas well	0.042
283	MBA	328	C5A	Oil well	0.000
284	BDL**	187	C7	Oil well	0.803
285	BDL**	183	C7	Oil well	0.459
286	BDL**	186	C7	Oil well	0.360
287	BDL**	197	C6	Oil well	0.250
288	BDL**	199	C6	Oil well	0.123
289	BDL**	182	C7	Oil well	0.112
290	BDL**	106	C7	Gas well	0.105
291	BDL**	196	C6	Oil well	0.080
292	BDL**	110	C8	Oil well	0.079
293	BDL**	112	C8	Gas well	0.079
294	BDL**	115	C8	Gas well	0.079
295	BDL**	184	C7	Gas well	0.051
296	BDL**	188	C7	Oil well	0.049
297	BDL**	117	C8	Gas well	0.039
298	BDL**	119	C8	Gas well	0.039
299	BDL**	121	C8	Gas well	0.039
300	BDL**	195	C6	Facility	0.033
301	BDL**	189	C7	Oil well	0.033
302	BDL**	131	C7	Oil well	0.030
303	BDL**	133	C7	Oil well	0.030
304	BDL**	134	C7	Oil well	0.030
305	BDL**	200	C6	Oil well	0.013
306	BDL**	103	C7	Oil well	0.012
307	BDL**	102	C6	Oil well	0.010
308	BDL**	185	C7	Oil well	0.009
309	BDL**	194	C6	Oil well	0.008
310	BDL**	108	C7	Oil well	0.007
311	BDL**	109	C7	Oil well	0.007
312	BDL**	113	C8	Gas well	0.006
313	BDL**	114	C8	Gas well	0.006
314	BDL**	104	C7	Oil well	0.006

315	BDL**	105	C7	Oil well	0.006
316	BDL**	107	C7	Oil well	0.006
317	BDL**	111	C8	Gas well	0.006
318	BDL**	192	C6	Oil well	0.004
319	BDL**	124	C8	Gas well	0.003
320	BDL**	125	C8	Gas well	0.003
321	BDL**	190	C7	Oil well	0.003
322	BDL**	127	C8	Gas well	0.003
323	BDL**	128	C8	Gas well	0.003
324	BDL**	129	C8	Gas well	0.003
325	BDL**	130	C7	Oil well	0.003
326	BDL**	132	C7	Oil well	0.002
327	BDL**	120	C8	Oil well	0.002
328	BDL**	122	C8	Oil well	0.002
329	BDL**	126	C8	Oil well	0.002
330	BDL**	191	C7	Oil well	0.001
331	BDL**	193	C6	Facility	0.001
332	BDL**	198	C6	Oil well	0.001
333	BDL**	123	C8	Facility	0.001
334	BDL**	99	C7	Gas well	0.001
335	BDL**	100	C5A	Oil well	0.001
336	BDL**	101	C5A	Oil well	0.001
337	BDL**	116	C8	Facility	0.000
338	BDL**	118	C8	Facility	0.000

*Emission rate for this site is the sum of quantified emissions from a group of three sites where their contribution to the measured emission plume could not be distinguished.

**BDL values are only used for the derivation of the detection limit and the fraction of non-detects for the TDM dataset. They are not used for the emission quantification.

References

Alvarez, R. A., Zavala-Araiza, D., Lyon, D. R., Allen, D. T., Barkley, Z. R., Brandt, A. R., Davis, K. J., Herndon, S. C., Jacob, D. J., Karion, A., Kort, E. A., Lamb, B. K., Lauvaux, T., Maasakkers, J. D., Marchese, A. J., Omara, M., Pacala, S. W., Peischl, J., Robinson, A. L., Shepson, P. B., Sweeney, C., Townsend-Small, A., Wofsy, S. C., and Hamburg, S. P.: Assessment of methane emissions from the U.S. oil and gas supply chain, Science, 361, 186–188, https://doi.org/10.1126/science.aar7204, 2018.

Bacharach, I. N. C.: Hi flowR sampler for natural gas leak rate measurement, 2015.

Canty, A. and Ripley, B.: boot: Bootstrap R (S-Plus) Functions., R package version 1.3-28, 2021.

Delre, A., Hensen, A., Velzeboer, I., van den Bulk, P., Edjabou, M. E., and Scheutz, C.: Methane and ethane emission quantifications from onshore oil and gas sites in Romania, using a tracer gas dispersion method, Elementa: Science of the Anthropocene, 10, 000111, https://doi.org/10.1525/elementa.2021.000111, 2022.

Hanna, S. R., Briggs, G. A., and Hosker, J.: Handbook on atmospheric diffusion, National Oceanic and Atmospheric Administration, Oak Ridge, TN (USA). Atmospheric Turbulence and Diffusion Lab., https://doi.org/10.2172/5591108, 1982.

Korbeń, P., Jagoda, P., Maazallahi, H., Kammerer, J., Nęcki, J. M., Wietzel, J. B., Bartyzel, J., Radovici, A., Zavala-Araiza, D., Röckmann, T., and Schmidt, M.: Quantification of methane emission rate from oil and gas wells in Romania using ground-based measurement techniques, Elementa: Science of the Anthropocene, 10, 00070, https://doi.org/10.1525/elementa.2022.00070, 2022.

Lyman, S. N., Tran, T., Mansfield, M. L., and Ravikumar, A. P.: Aerial and ground-based optical gas imaging survey of Uinta Basin oil and gas wells, Elementa: Science of the Anthropocene, 7, 43, https://doi.org/10.1525/elementa.381, 2019.

Razali, N. M. and Wah, Y. B.: Power comparisons of shapiro-wilk, kolmogorov-smirnov, lilliefors and anderson-darling tests, Journal of statistical modeling and analytics, 2, 21–33, 2011.

Riddick, S. N., Connors, S., Robinson, A. D., Manning, A. J., Jones, P. S. D., Lowry, D., Nisbet, E., Skelton, R. L., Allen, G., Pitt, J., and Harris, N. R. P.: Estimating the size of a methane emission point source at different scales: from local to landscape, Atmospheric Chemistry and Physics, 17, 7839–7851, https://doi.org/10.5194/acp-17-7839-2017, 2017.

Robertson, A. M., Edie, R., Field, R. A., Lyon, D., McVay, R., Omara, M., Zavala-Araiza, D., and Murphy, S. M.: New Mexico Permian Basin Measured Well Pad Methane Emissions Are a Factor of 5–9 Times Higher Than U.S. EPA Estimates, Environ. Sci. Technol., 54, 13926–13934, https://doi.org/10.1021/acs.est.0c02927, 2020.

Ruckstuhl, A. F., Henne, S., Reimann, S., Steinbacher, M., Vollmer, M. K., O'Doherty, S., Buchmann, B., and Hueglin, C.: Robust extraction of baseline signal of atmospheric trace species using local regression, Atmospheric Measurement Techniques, 5, 2613–2624, https://doi.org/10.5194/amt-5-2613-2012, 2012.

Seabold, S. and Perktold, j: statsmodels: Econometric and statistical modeling with python, 9th Python in Science Conference., 2010.

Turner, D.: Workbook of atmospheric dispersion estimates (Office of Air Program Pub. No. AP-26), Washington, DC: Environmental Protection Agency, 1970.

Vinković, K., Andersen, T., de Vries, M., Kers, B., van Heuven, S., Peters, W., Hensen, A., van den Bulk, P., and Chen, H.: Evaluating the use of an Unmanned Aerial Vehicle (UAV)-based active AirCore system to quantify methane emissions from dairy cows, Science of The Total Environment, 831, 154898, https://doi.org/10.1016/j.scitotenv.2022.154898, 2022.

Virtanen, P., Gommers, R., Oliphant, T. E., Haberland, M., Reddy, T., Cournapeau, D., Burovski, E., Peterson, P., Weckesser, W., Bright, J., van der Walt, S. J., Brett, M., Wilson, J., Millman, K. J., Mayorov, N., Nelson, A. R. J., Jones, E., Kern, R., Larson, E., Carey, C. J., Polat, İ., Feng, Y., Moore, E. W., VanderPlas, J., Laxalde, D., Perktold, J., Cimrman, R., Henriksen, I., Quintero, E. A., Harris, C. R., Archibald, A. M., Ribeiro, A. H., Pedregosa, F., van Mulbregt, P., SciPy 1.0 Contributors, Vijaykumar, A., Bardelli, A. P., Rothberg, A., Hilboll, A., Kloeckner, A., Scopatz, A., Lee, A., Rokem, A., Woods, C. N., Fulton, C., Masson, C., Häggström, C., Fitzgerald, C., Nicholson, D. A., Hagen, D. R., Pasechnik, D. V., Olivetti, E., Martin, E., Wieser, E., Silva, F., Lenders, F., Wilhelm, F., Young, G., Price, G. A., Ingold, G.-L., Allen, G. E., Lee, G. R., Audren, H., Probst, I., Dietrich, J. P., Silterra, J., Webber, J. T., Slavič, J., Nothman, J., Buchner, J., Kulick, J., Schönberger, J. L., de Miranda Cardoso, J. V., Reimer, J., Harrington, J., Rodríguez, J. L. C., Nunez-Iglesias, J., Kuczynski, J., Tritz, K., Thoma, M., Newville, M., Kümmerer, M., Bolingbroke, M., Tartre, M., Pak, M., Smith, N. J., Nowaczyk, N., Shebanov, N., Pavlyk, O., Brodtkorb, P. A., Lee, P., McGibbon, R. T., Feldbauer, R., Lewis, S., Tygier, S., Sievert, S., Vigna, S., Peterson, S., More, S., et al.: SciPy 1.0: fundamental algorithms for scientific computing in Python, Nat Methods, 17, 261–272, https://doi.org/10.1038/s41592-019-0686-2, 2020.

Yacovitch, T. I., Herndon, S. C., Pétron, G., Kofler, J., Lyon, D., Zahniser, M. S., and Kolb, C. E.: Mobile Laboratory Observations of Methane Emissions in the Barnett Shale Region, Environ. Sci. Technol., 49, 7889–7895, https://doi.org/10.1021/es506352j, 2015.

Zavala-Araiza, D., Lyon, D. R., Alvarez, R. A., Davis, K. J., Harriss, R., Herndon, S. C., Karion, A., Kort, E. A., Lamb, B. K., Lan, X., Marchese, A. J., Pacala, S. W., Robinson, A. L., Shepson, P. B., Sweeney, C., Talbot, R., Townsend-Small, A., Yacovitch, T. I., Zimmerle, D. J., and Hamburg, S. P.: Reconciling divergent estimates of oil and gas methane emissions, Proceedings of the National Academy of Sciences, 112, 15597–15602, https://doi.org/10.1073/pnas.1522126112, 2015.

Zavala-Araiza, D., Herndon, S. C., Roscioli, J. R., Yacovitch, T. I., Johnson, M. R., Tyner, D. R., Omara, M., and Knighton, B.: Methane emissions from oil and gas production sites in Alberta, Canada, Elementa: Science of the Anthropocene, 6, 27, https://doi.org/10.1525/elementa.284, 2018.